Small-Molecule Planar-Mixed Heterojunction Photovoltaic Cells with Fullerene-Based Electron Filtering Buffers

*Xin Xiao, Kevin J. Bergemann, Jeramy D. Zimmerman, Kyusang Lee, and Stephen R. Forrest**

Small-molecule organic photovoltaic (OPV) cells have attracted interest due to their promise for use as low-cost, light-weight, and flexible renewable energy sources.[1–9] Among the various device architectures currently being explored, small-molecule-based hybrid planar-mixed heterojunctions (PM-HJ) have advantages over conventional planar junctions, including strong absorption, efficient exciton dissociation, and long-term reliability.[7,10,11] Previously, we demonstrated an efficient PM-HJ OPV based on tetraphenyldibenzoperiflanthene (DBP)[12–14] as a donor and C_{70} as an acceptor with a power conversion efficiency of $PCE = 6.4\% \pm 0.3\%$ under simulated AM 1.5G illumination at 1 sun intensity.[7] Despite its high short-circuit current density (J_{SC}) and open-circuit voltage (V_{OC}), the DBP:C_{70} PM-HJ OPV cell suffers from a relatively low fill factor of $FF = 56\% \pm 1\%$, suggesting that there remains considerable room for performance improvement. Here, we demonstrate PM-HJ OPV cells employing fullerene-based compound cathode buffer layers that block excitons while efficiently conducting electron-polarons, thereby acting as an "electron filter" that results in reduced bimolecular recombination and exciton-polaron quenching. The compound buffer consists of a blend of wide energy-gap, exciton-blocking bathophenanthroline (BPhen) and electron conducting C_{60} capped with a neat BPhen layer. The compound buffer significantly increases *FF* in the PM-HJ to $66\% \pm 1\%$. Hence, the OPV with a compound buffer achieves $PCE = 8.1\% \pm 0.4\%$ under simulated AM 1.5G, 1 sun illumination. Furthermore, the responsivity, $R = J_{SC}/I$, where I is the incident light intensity, of the control monotonically decreases with light intensity in contrast to the cell with a BPhen:C_{60}/BPhen electron-filtering buffer whose responsivity is nearly constant over the same light intensities, providing further evidence that both bimolecular recombination and exciton-polaron quenching are suppressed.

X. Xiao, Dr. J. D. Zimmerman, K. Lee, Prof. S. R. Forrest
Department of Electrical Engineering
and Computer Science
University of Michigan
Ann Arbor, MI, 48109, USA
E-mail: stevefor@umich.edu
K. J. Bergemann, Prof. S. R. Forrest
Department of Physics
University of Michigan
Ann Arbor, MI, 48109, USA
Prof. S. R. Forrest
Department of Materials Science and Engineering
University of Michigan
Ann Arbor, MI, 48109, USA

DOI: 10.1002/aenm.201301557

In the PM-HJ structure, there are two principal loss mechanisms leading to the low *FF*. One is bimolecular recombination of free charge carriers in the extensive donor-acceptor blended region of the PM-HJ structure,[15,16] whose rate is given by $k_{BM} = \gamma np$. Here, γ is the Langevin recombination constant, and $n(p)$ is the free electron (hole) density. A second significant loss is due to exciton-polaron quenching in the neat C_{70} layer.[17,18] In previous work,[19] electron-polaron build-up was observed at the neat acceptor/blocking layer interface that results in quenching and, therefore, a reduction of internal quantum efficiency (*IQE*). Note that exciton-polaron quenching follows a similar relationship to bimolecular recombination, as both exciton and polaron concentrations are proportional to intensity. Both mechanisms can result in a loss in photocurrent under forward bias that increases the slope of current density–voltage (*J–V*) characteristics in the fourth quadrant, ultimately decreasing both *FF* and *PCE*.

Recently, an electron conducting/exciton blocking fullerene-based mixed buffer layer placed adjacent to the cathode was shown to increase the efficiency of bilayer OPV cells.[19] The buffer consists of a mixture of C_{60} that efficiently conducts electron-polarons and wide energy gap bathocuproine (BCP) that blocks excitons. Exciton-polaron quenching was significantly reduced in bilayer cells employing this electron filter due to its ability to spatially separate excitons and polarons at the blocking interface. This led to a significant increase in J_{SC}, while V_{OC} and *FF* remained unchanged. The PM-HJ cells additionally suffer from bimolecular recombination in the mixed photoactive layer. Using a mixed buffer results in a reduced interfacial field with the active layer due to its increased conductivity compared to a neat, conventional blocking buffer layer.[19] The resulting increase in field across the photosensitive region leads to more rapid charge extraction. This, in turn, leads to reduced bimolecular recombination in the cell.

To disaggregate the sources of loss, we employ the BPhen:C_{60} mixed buffer with only a DBP:C_{70} mixed HJ as the photoactive region to determine the effects of bimolecular recombination alone. In this structure, excitons rapidly dissociate into charge carriers within the DBP:C_{70} blend.[7] The exciton concentration is negligible in the mixed layer, thereby eliminating exciton-polaron quenching as a significant loss mechanism.

The mixed HJ cells were grown by vacuum thermal evaporation (VTE) with the structure: MoO_3 (10 nm)/DBP:C_{70} (54 nm, 1:8 volume ratio)/buffer/Ag (100 nm). Two different buffer layers were employed: 8 nm-thick BPhen (control), and 10 nm-thick BPhen:C_{60} mixed layer at 1:1 ratio (by volume) capped with a neat, 5 nm-thick BPhen layer. **Figure 1**a,b show the *J–V* characteristics and *EQE* spectra of mixed HJ devices

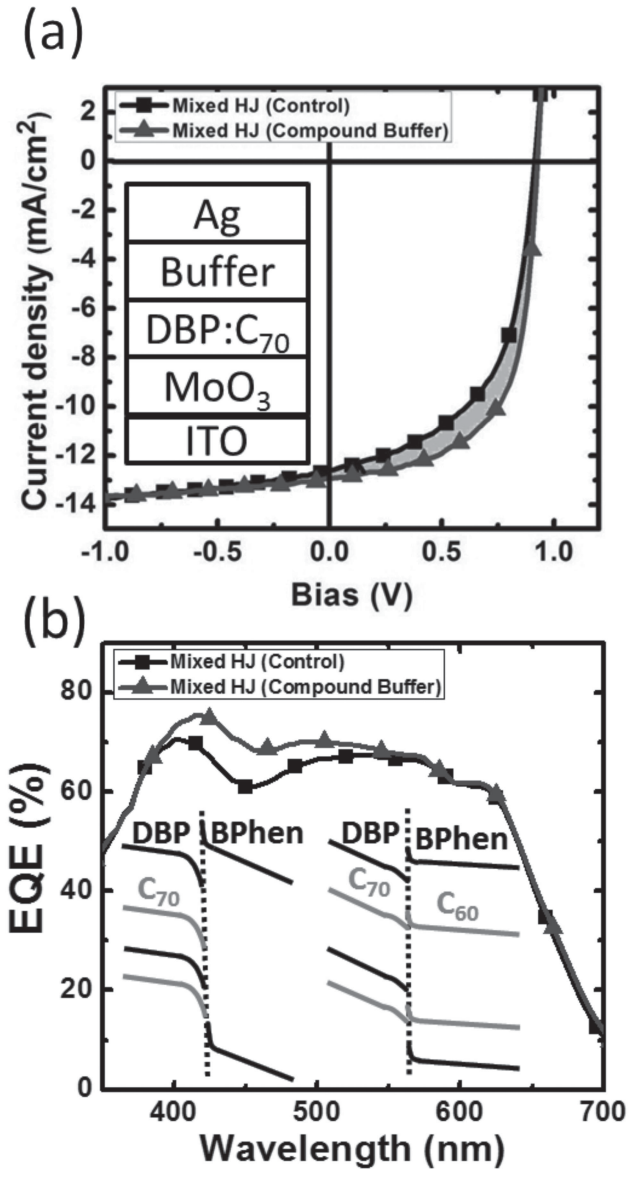

Figure 1. a) Spectrally corrected *J–V* characteristics under simulated AM 1.5G, 1 sun illumination for DBP:C_{70} mixed-HJ OPV cells. The shaded region emphasizes the difference in fill factors, and hence maximum power output, of the two cells. Inset: Schematic of the device structure. b) *EQE* spectra for the cells in (a). Inset: Schematic diagrams of energy levels at the DBP:C_{70}/buffer interface (left: neat BPhen buffer; right: BPhen:C_{60} compound buffer).

employing the control and compound buffers. The control has $FF = 55\% \pm 1\%$, $J_{SC} = 12.5 \pm 0.3$ mA cm^{-2}, $V_{OC} = 0.91 \pm 0.1$ V and $PCE = 6.3\% \pm 0.3\%$ under simulated AM 1.5G, 1 sun illumination (spectral mismatch factor[20] = 1.00 ± 0.01), as previously.[7] The cells with the compound electron-filter buffer exhibit improvement in all three performance parameters, leading to $FF = 63\% \pm 1\%$, $J_{SC} = 12.8 \pm 0.3$ mA cm^{-2}, $V_{OC} = 0.93 \pm 0.1$ V and $PCE = 7.5\% \pm 0.4\%$, the latter corresponding to a 19% increase compared to the control.

The significant improvement in *FF* for the device with the compound buffer is shown in Figure 1a (indicated by the shaded region between the curves) with the energy level diagram in Figure 1b (inset). Previous studies have shown that energy level bending occurs at the fullerene/BCP interface,[21,22] leading to electron accumulation and a large potential drop as shown in the left inset. Consequently, the field across the active layers is reduced as the voltage is redistributed, increasing the charge extraction time and, therefore, the residence time for electrons and holes at the donor-acceptor heterointerface where they have an opportunity to recombine. In the case of the compound buffer, the high conductivity of the 1:1 BPhen:C_{60} blend[19] results in less electron accumulation and, therefore, a smaller potential drop at the interface (right inset, Figure 1b) and a higher electric field in the DBP:C_{70} mixed region. This in turn leads to reduced bimolecular quenching and consequently an increased *FF* and *EQE* at wavelengths between $\lambda = 400$ nm and 550 nm, as shown in Figure 1b.

Both cells show almost identical *EQE* at $\lambda < 400$ nm and $\lambda > 550$ nm (Figure 1b). At $\lambda < 400$ nm, the photoactive region absorption decreases in the compound buffer cell resulting from parasitic absorption in the BPhen:C_{60} mixed buffer[19] while the internal quantum efficiency (*IQE*) increases due to reduced bimolecular recombination. Overall, the *EQE* of the compound buffer cell is nearly equal to the control cell. At $\lambda > 550$ nm, the absorbed optical power peak as well as charge distribution peak shift towards the anode, since the excitons generated in the DBP:C_{70} mixed region almost immediately dissociate into charges. This reduces the population of holes at the DBP:C_{70}/BPhen interface (close to the cathode side) where electrons pile up in the control cell, while at the same time improving hole extraction. The spatial separation of the holes and electrons at longer excitation wavelengths reduces bimolecular recombination in the control cell, leading to the almost identical *EQE* as well.

To understand the role of bimolecular recombination, we investigated the responsivity (R) for both cells as a function of light intensity (I). The control cell is found to have a monotonic decrease in R with I, from $R = (12.7 \pm 0.4) \times 10^{-2}$ A W^{-1} at $I = 0.6$ sun, to $(11.8 \pm 0.3) \times 10{-}^{2}$ A W^{-1} at $I = 2.7$ suns, while for the compound buffer cell, R drops by only 0.002 A W^{-1} over the same range of intensities (see **Figure 2**). In general, $J_{SC} = J_G - J_{MM} - J_{BM}$, where J_G is the photogenerated current density, J_{MM} is the monomolecular recombination current density and J_{BM} is the bimolecular recombination current density. Both J_G and J_{MM} are linearly proportional to I, while $J_{BM} \propto \gamma np \propto \beta I^2$, where γ is the Langevin coefficient and β is a constant. Therefore, $R = J_{SC}/I = R_0 - \beta I$, where R_0 is the responsivity in the absence of bimolecular recombination. The linear fits to this analysis (dashed lines, Figure 2) yields $R_0 = 12.9$ A W^{-1} for both cells. The same intercept for both cells at zero light intensity suggests that they have the same responsivities as $I \rightarrow 0$ in the absence of bimolecular recombination. However, β for the control is four times larger than that for the cell with the compound buffer. The smaller β for the compound buffer cell suggests that bimolecular recombination is only 25% of that of the control cell, indicating that the electron and hole concentrations have each decreased, on average, by 50% due to the increased electric field in the mixed region. This larger internal field across the heterojunction in the compound buffer cell compared to that of the control for a

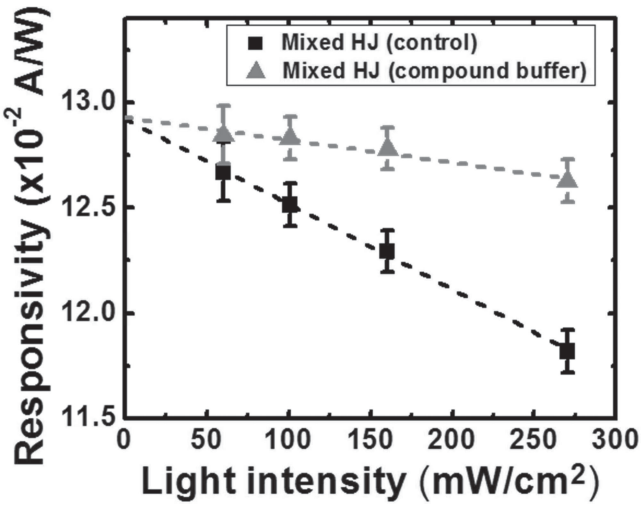

Figure 2. Responsivity vs. light intensity for the mixed-HJ control cell and the compound buffer cell with linear fits according to bimolecular recombination theory (dashed lines).[15,16]

given external bias results in improved charge extraction and, therefore, higher *FF*.

The charge transport properties of the compound buffer were further investigated by 3D Monte Carlo simulations of the layer, programmed in MATLAB. The buffer was modeled as a random distribution of BPhen and C_{60} molecules on a cubic lattice, with electron transport attributed to nearest-neighbor hopping between C_{60} molecules. In this model, Columbic interactions between charges are neglected, and the lattice sites are assumed to be isoenergetic, aside from energy differences imposed by the applied electric field. Transfer probabilities were calculated according to Miller–Abrahams theory,[23–27] from which the median extraction time for charges injected on one side of the buffer layer was obtained. The mobility of the layer was then calculated from the relationship between extraction time and electric field, normalized by setting the zero-field mobility of electrons in the neat C_{60} layer to the experimental value of 5.1×10^{-2} cm^2 V^{-1} s^{-1}.[28] For a 1:1 mixed buffer, the model predicts an effective mobility of 4.7×10^{-3} cm^2 V^{-1} s^{-1}, only one order of magnitude lower than that of neat C_{60}. In comparison, the neat BPhen film has a significantly lower electron mobility of 1.9×10^{-5} cm^2 V^{-1} s^{-1},[29] leading to charge pile-up at the buffer interface that promotes quenching.

The model was tested by examining the predictions for different thicknesses of a 1:1 mixed buffer, with the results in **Figure 3**a. We find a linear relationship between extraction time (corresponding to film mobility) at a given voltage and thickness of the mixed layers, which translates to a linear increase in series resistance, assuming a constant charge density (i.e., a constant illumination intensity). Fits to the experimental data for mixed buffer DBP:C_{60} OPVs are shown in Figure 3a (inset). Now, a neat BPhen layer that conducts electrons through defect states induced during metal deposition, thereby leading to a superlinear relationship between thickness and resistance.[30] In contrast, the mixed buffer resistance increases linearly with thickness even up 20 nm, suggesting that electrons in the mixed buffer are predominantly conducted by the C_{60} in the mixture

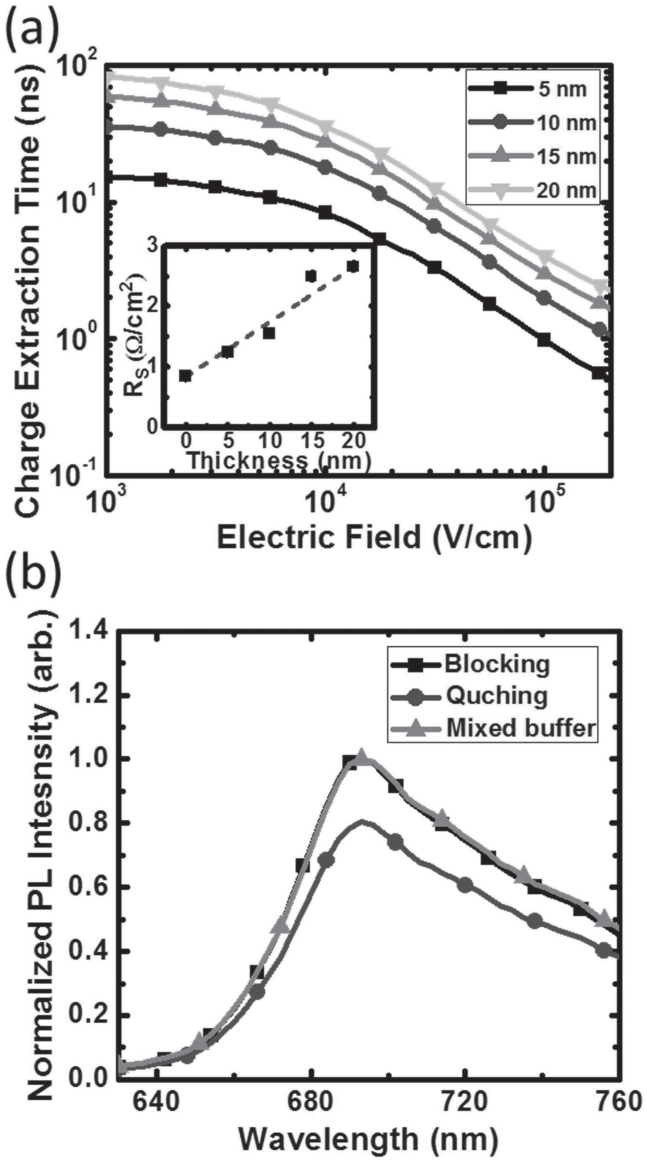

Figure 3. a) Charge extraction time vs. electric field for various layer thicknesses calculated using 3D Monte-Carlo simulations. Inset: Cell series resistance (R_S) vs. layer thickness with a linear fit (dashed line) to the data obtained from the OPV cells (squares). Error bars in the inset are smaller than data points. b) PL spectra for a neat C_{70} layer in contact with BPhen (blocking), NPD (quenching) and BPhen:C_{60} mixed layers obtained at an excitation wavelength of $\lambda = 520$ nm.

Previously, we showed that the 1:1 BCP:C_{60} blend has an 81% exciton-blocking efficiency using 3D Monte Carlo simulations.[19] Here, we experimentally investigate its exciton blocking efficiency using the photoluminescence (PL) excitation spectra of a 40 nm-thick C_{70} film capped with a 1:1 BPhen:C_{60} blend on quartz.[31] By comparing the PL intensity of the layer deposited onto the surface of the blend under study to that of either a "perfectly" blocking or quenching layer, the relative importance of these processes can be determined. For this comparison, therefore, an 8 nm-thick BPhen or *N,N′*-diphenyl-*N,N′*-bis(1-naphthyl)-1–1′-biphenyl-4,4′diamine (NPD) layer are used as

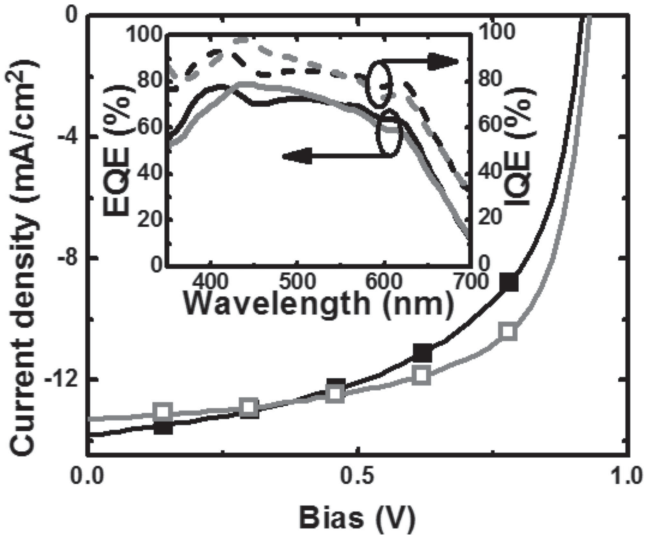

Figure 4. Spectrally corrected *J–V* characteristics under simulated AM 1.5G, 1 sun illumination for DBP:C_{70} PM-HJ OPV cells with a neat BPhen buffer (solid squares) and a compound buffer (hollow squares). Inset: *EQE* (solid lines) and *IQE* (dashed lines) spectra for the control (black) and the compound buffer cell (gray).

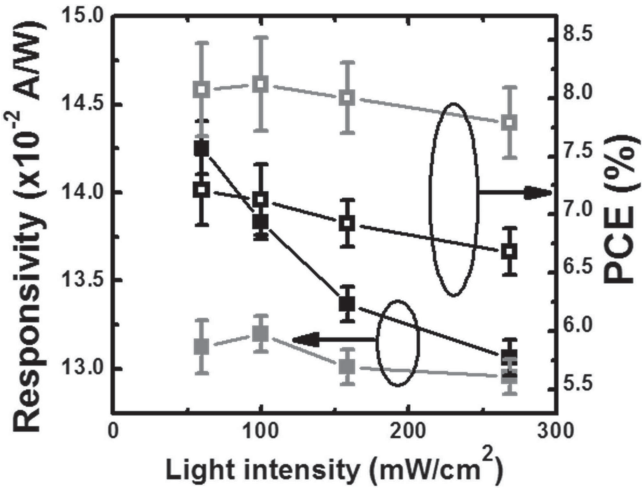

Figure 5. Responsivity (solid squares) and power conversion efficiency (*PCE*) (hollow squares) vs. light intensity for the PM-HJ control cell (black symbols), and the cell with a BPhen:C_{60}/BPhen compound buffer (gray symbols).

reference, one as a perfectly exciton blocking and the other as a quenching layer,[31] respectively. The PL intensity of the mixed buffer is nearly identical to the intensity found for the blocking reference (Figure 3b), demonstrating that BPhen:C_{60} mixed layer can efficiently block excitons. Since BPhen:C_{60} mixture has a relatively high electron mobility, the mixed buffer layer can spatially separate excitons and polarons acting as an effective filter, leading to a reduction of exciton-polaron quenching within the neat fullerene layer.

The DBP:C_{70} PM-HJ OPV exploits the advantages of the mixed buffer by employing it adjacent to a neat C_{70} layer using the following structure: indium tin oxide (ITO)/MoO_3 (10 nm)/ DBP:C_{70} (54 nm, 1:8)/C_{70} (9 nm)/buffer/Ag (100 nm). **Figure 4** shows the *J–V* characteristics and *EQE* spectra (inset) of the cells with both the control and compound buffers. The control has $PCE = 7.1\% \pm 0.3\%$, which is comparable to previous results.[7] The compound buffer results in a nearly 20% increase in *FF* to $66\% \pm 1\%$, as anticipated for architectures with reduced recombination of photogenerated carriers. Also, $V_{OC} = 0.93 \pm 0.1$ V for the compound buffer compared with 0.91 ± 0.1 V for the control, and J_{SC} decreases to 13.2 ± 0.3 mA cm^{-2} from 13.8 ± 0.3 mA cm^{-2} for the control due to the reduced *EQE* in the range $\lambda < 420$ nm and $\lambda > 550$ nm. Overall, the OPV cell with a BPhen:C_{60}/BPhen buffer exhibits $PCE = 8.1\% \pm 0.4\%$ under simulated AM 1.5G, 1 sun illumination, which is among the highest efficiencies reported for VTE-grown OPV cells. The *EQE* and the internal quantum efficiency (*IQE*) spectra[32,33] of the mixed buffer and control cells are shown in the inset, Figure 4. The compound buffer cell shows an increased *EQE* between $\lambda = 420$ nm and 550 nm, while *EQE* decreases outside of this range for the compound buffer cell compared to the control. Similar to the case of the mixed HJ, the reduced *EQE* for the compound buffer cell at $\lambda < 420$ nm is due to the absorption of the BPhen:C_{60} mixed buffer. At $\lambda > 550$ nm, the peak absorbed optical power in the control shifts closer to the anode than for the compound buffer cell, which enhances the hole extraction and, therefore, reduces bimolecular recombination in the control. At $\lambda > 550$ nm, the absorbed optical power in the neat C_{70} layer in the control is lower than that in the compound buffer due to the optical peak moving farther from the cathode, leading to the reduced exciton-polaron quenching in the control. Therefore, the *EQE* for the control is higher than that for the compound buffer cell at $\lambda > 550$ nm.

The *IQE* of the compound buffer cell averages ≈90% between $\lambda = 350$ nm and 500 nm while the *IQE* in the control averages only ≈80% over the same spectrum range. The *IQE* increase results from a reduction in both bimolecular recombination and exciton-polaron quenching for the case of the mixed buffer.

The intensity dependence of *R* and *PCE* for both cells ranging from 0.6 sun to 2.7 sun is shown in **Figure 5**. Similar to mixed HJ cells, the responsivity of the control cell decreases monotonically by 10%, from $R = (14.3 \pm 0.4) \times 10^{-2}$ A W^{-1} at 0.6 sun to $(13.0 \pm 0.4) \times 10^{-2}$ A W^{-1} at 2.7 sun. In contrast, the PM-HJ cell with the compound buffer shows only a 1.3% reduction with intensity. The significant drop in *R* of the control indicates substantial bimolecular recombination and exciton-polaron quenching, whereas these effects are significantly suppressed in the compound buffer cell.

In conclusion, we have demonstrated that the BPhen:C_{60}/Bphen compound buffer acts as an electron filter characterized by a high electron conductivity while efficiently blocking excitons. This combination of physical properties from the compound buffer prevents the build-up of charge at the active region/buffer interface even at very high illumination intensities, thereby suppressing losses from both bimolecular recombination and exciton-polaron quenching. The DBP:C_{70} PM-HJ cell with a compound buffer achieves $PCE = 8.1\% \pm 0.4\%$ with $FF = 66\% \pm 1\%$ under simulated AM 1.5G, 1 sun illumination.

Experimental Section

The OPV cells were grown by vacuum thermal evaporation (VTE) at a base pressure of 2×10^{-7} torr on glass substrates pre-coated with ITO (sheet resistance: 15 Ω $\square^{-1}$). Prior to deposition, the substrates were cleaned in diluted Tergitol (Type NP-10), deionized water, acetone, and isopropyl alcohol,[34] and then exposed to ultraviolet-ozone for 10 min. We obtained MoO_3 from Acros Organics, C_{60} from Materials and Electrochemical Research Corp., BPhen and DBP from Luminescence Technology Corp., and C_{70} from SES Research. DBP, C_{60} and C_{70} were purified once via thermal gradient sublimation.[35] The MoO_3 and BPhen layers were grown at a rate of 0.1 nm s^{-1}, DBP and C_{70} were co-deposited using a DBP deposition rate of 0.02 nm s^{-1} and a C_{70} deposition rate of 0.16 nm s^{-1} to achieve a 1:8 ratio. The BPhen:C_{60} mixed buffer was grown by co-depositing BPhen and C_{60} each at a rate of 0.05 nm s^{-1} creating a 1:1 blend. A 100 nm-thick Ag cathode was subsequently deposited through a shadow mask defining an array of 15, 1 mm diameter devices (device area of 0.008 cm^2). Following fabrication, devices were transferred into a glovebox filled with ultrahigh purity N_2 for measurement of the *J–V* characteristics and *EQE*. During measurement, only the tested device was under illumination while other devices were kept in the dark. The solar simulator intensities were calibrated using a NREL-traceable Si reference cell, and J_{SC} was corrected for spectral mismatch.[20] The *EQE* as a function of wavelength (λ) was obtained with a lock-in amplifier and monochromated light from a Xe-lamp chopped at 200 Hz. Errors in J_{SC} and *PCE* arose primarily from uncertainties in light intensity and spectral calibration.

Acknowledgements

The authors gratefully acknowledge C. K. Renshaw for helpful discussions. This work was partially supported by the Center for Solar and Thermal Energy Conversion at the University of Michigan, a Department of Energy, Energy Frontier Research Center, Award No. DE-SC0000957 (K.J.B., analysis; K.L., experiment), the SunShot NextGen II Program of the Department of Energy (X.X., experiment, analysis; S.R.F., analysis), and NanoFlex Power Corp. (J.D.Z., analysis).

Received: October 13, 2013
Revised: November 3, 2013
Published online: December 23, 2013

[1] A. Mishra, P. Bauerle, *Angew. Chem. Int. Ed.* **2012**, *51*, 2020.
[2] G. Chen, H. Sasabe, Z. Q. Wang, X. F. Wang, Z. R. Hong, Y. Yang, J. J. Kido, *Adv. Mater.* **2012**, *24*, 2768.
[3] A. K. K. Kyaw, X. W. Sun, C. Y. Jiang, G. Q. Lo, D. W. Zhao, D. L. Kwong, *Appl. Phys. Lett.* **2008**, *93*, 221107.
[4] B. E. Lassiter, J. D. Zimmerman, A. Panda, X. Xiao, S. R. Forrest, *Appl. Phys. Lett.* **2012**, *101*, 063303.
[5] R. Pandey, Y. L. Zou, R. J. Holmes, *Appl. Phys. Lett.* **2012**, *101*, 033308.
[6] X. Xiao, G. D. Wei, S. Y. Wang, J. D. Zimmerman, C. K. Renshaw, M. E. Thompson, S. R. Forrest, *Adv. Mater.* **2012**, *24*, 1956.
[7] X. Xiao, J. D. Zimmerman, B. E. Lassiter, K. J. Bergemann, S. R. Forrest, *Appl. Phys. Lett.* **2013**, *102*, 073302.
[8] G. D. Wei, X. Xiao, S. Y. Wang, K. Sun, K. J. Bergemann, M. E. Thompson, S. R. Forrest, *ACS Nano* **2012**, *6*, 972.
[9] J. D. Zimmerman, B. E. Lassiter, X. Xiao, K. Sun, A. Dolocan, R. Gearba, D. A. V. Bout, K. J. Stevenson, P. Wickramasinghe, M. E. Thompson, S. R. Forrest, *ACS Nano* **2013**, *7*, 9268.
[10] J. G. Xue, B. P. Rand, S. Uchida, S. R. Forrest, *Adv. Mater.* **2005**, *17*, 66.
[11] X. T. Tong, N. Wang, M. Slootsky, J. Yu, S. R. Forrest, *Sol. Energ. Mater. Sol. Cells* **2013**, *118*, 116.
[12] M. Hirade, C. Adachi, *Appl. Phys. Lett.* **2011**, *99*, 153302.
[13] D. Fujishima, H. Kanno, T. Kinoshita, E. Maruyama, M. Tanaka, M. Shirakawa, K. Shibata, *Sol. Energy Mater. Sol. Cells* **2009**, *93*, 1029.
[14] D. Yokoyama, Z. Q. Wang, Y. J. Pu, K. Kobayashi, J. Kido, Z. R. Hong, *Sol. Energy Mater. Sol. Cells* **2012**, *98*, 472.
[15] A. K. Kyaw, D. H. Wang, V. Gupta, W. L. Leong, L. Ke, G. C. Bazan, A. J. Heeger, *ACS Nano* **2013**, *7*, 4569.
[16] L. J. A. Koster, V. D. Mihailetchi, P. W. M. Blom, *Appl. Phys. Lett.* **2006**, *88*, 052104.
[17] B. Verreet, P. E. Malinowski, B. Niesen, D. Cheyns, P. Heremans, A. Stesmans, B. P. Rand, *Appl. Phys. Lett.* **2013**, *102*, 043301.
[18] J. M. Hodgkiss, S. Albert-Seifried, A. Rao, A. J. Barker, A. R. Campbell, R. A. Marsh, R. H. Friend, *Adv. Funct. Mater.* **2012**, *22*, 1567.
[19] A. N. Bartynski, C. Trinh, A. Panda, K. Bergemann, B. Lassiter, J. D. Zimmerman, S. R. Forrest, M. E. Thompson, *Nano Lett.* **2013**, *13*, 3315.
[20] C. H. Seaman, *Sol. Energy* **1982**, *29*, 291.
[21] S. H. Wang, T. Sakurai, R. Kuroda, K. Akimoto, *Appl. Phys. Lett.* **2012**, *100*, 243301.
[22] J. X. Tang, Y. C. Zhou, Z. T. Liu, C. S. Lee, S. T. Lee, *Appl. Phys. Lett.* **2008**, *93*, 043512.
[23] A. Miller, E. Abrahams, *Phys. Rev.* **1960**, *120*, 745.
[24] H. Bassler, *Phys. Status Solidi B* **1993**, *175*, 15.
[25] I. I. Fishchuk, D. Hertel, H. Bässler, A. K. Kadashchuk, *Phys. Rev. B* **2002**, *65*.
[26] A. B. Walker, A. Kambili, S. J. Martin, *J. Phys.: Condens. Matter* **2002**, *14*.
[27] U. Wolf, V. I. Arkhipov, H. Bässler, *Phys. Rev. B* **1999**, *59*, 7507.
[28] B. P. Rand, J. G. Xue, S. Uchida, S. R. Forrest, *J. Appl. Phys.* **2005**, *98*, 124902.
[29] M. A. Khan, W. Xu, Khizar-ul-Haq, Y. Bai, X. Y. Jiang, Z. L. Zhang, W. Q. Zhu, Z. L. Zhang, W. Q. Zhu, *J. Appl. Phys.* **2008**, *103*, 014509.
[30] P. Peumans, S. R. Forrest, *Appl. Phys. Lett.* **2001**, *79*, 126.
[31] K. J. Bergemann, S. R. Forrest, *Appl. Phys. Lett.* **2011**, *99*, 243303.
[32] L. A. A. Pettersson, L. S. Roman, O. Inganas, *J. Appl. Phys.* **1999**, *86*, 487.
[33] P. Peumans, A. Yakimov, S. R. Forrest, *J. Appl. Phys.* **2004**, *95*, 2938.
[34] F. Yang, K. Sun, S. R. Forrest, *Adv. Mater.* **2007**, *19*, 4166.
[35] S. R. Forrest, *Chem. Rev.* **1997**, *97*, 1793.